Controlled Intracellular Release of Doxorubicin in Multidrug-Resistant Cancer Cells by Tuning the Shell-Pore Sizes of Mesoporous Silica Nanoparticles

Yu Gao,[†,§] Yu Chen,[‡,§] Xiufeng Ji,[†,§] Xinyu He,[†] Qi Yin,[†] Zhiwen Zhang,[†] Jianlin Shi,[‡,*] and Yaping Li[†,*]

[†]Shanghai Institute of Materia Medica, Chinese Academy of Sciences, 501 Haike Road, Shanghai 201203, People's Republic of China, and [‡]State Key Laboratory of High Performance Ceramics and Superfine Microstructure, Shanghai Institute of Ceramics, Chinese Academy of Sciences, 1295 Dingxi Road, Shanghai 200050, People's Republic of China. [§]These authors contributed equally to this work.

ABSTRACT

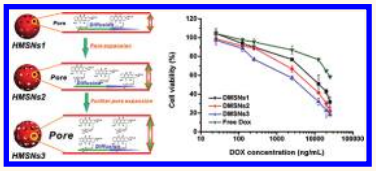

In this work, hollow mesoporous silica nanoparticles (HMSNs) with three pore sizes were manufactured to control the drug release rate, and the biological roles of these HMSNs were evaluated in multidrug-resistant (MDR) cancer cells. As novel pore-size-controllable inorganic materials, HMSNs showed negligible cytotoxicity and efficient cellular uptake toward drug-sensitive MCF-7 and drug-resistant MCF-7/ADR cells. Doxorubicin (DOX)-loaded HMSNs (DMSNs) not only demonstrated effective drug loading and a pH-responsive drug release character but also exhibited pore-size-dependent and sustained drug release performance in both *in vitro* and intracellular drug release experiments. In addition, DMSNs exhibited pore-size-dependent anticancer activity against MCF-7/ADR cells. DMSNs with larger pore size could mediate more cellular uptake of DOX and faster intracellular drug release, which led to more intracellular drug accumulation and stronger MDR-reversal effects. The MDR-overcoming mechanism could be due to the efficient cellular uptake, P-gp inhibition, and ATP depletion. These results demonstrate that HMSNs could be a very promising drug delivery system for pore-size-controllable drug release and cancer MDR reversion.

KEYWORDS: multidrug resistance · hollow mesoporous silica nanoparticles · pore size · drug delivery · doxorubicin

The development of multidrug resistance (MDR) is one of the main obstacles to effective cancer treatment.[1] Although great efforts have been made to overcome MDR, only limited success was achieved in clinical use;[2] for example, high-dose regimens were effective in some cases, but were often accompanied with increased toxicity,[3] and new chemotherapeutic drugs or their combination with chemosensitizing agents also was discouraging in clinical application.[4−6] In addition, it was reported that the effective control of drug release rate was very important for personal treatment because different stages of disease evolution usually need specific drug release rates.[7] In particular, the development of MDR of tumor cells is a multistep process, and MDR tumor cells at different stages or with different mechanisms require different drug exposure time and different treatment concentration.[8,9] The presence of a drug delivery system (DDS) with suitable release rate and release period of drug could lead to optimal clinical outcomes in cancer therapy. Unfortunately, it still is a big challenge to elaborately design drug carriers with the desired drug release rate to effectively overcome MDR.

Organic DDSs, such as drug-loaded polymeric capsules, have been employed to enhance the intracellular drug concentrations in the drug-resistant cells.[10] However, the low drug encapsulation efficiency and chemical/thermal instability of these organic DDSs have severely impeded their further clinical use. Compared to traditional organic DDSs, DDSs based on inorganic bionanomaterials showed great potential to overcome MDR because of their intrinsic high stability, excellent biocompatibility, and good degradability;[11,12] in particular, hollow nanostructured materials with well-defined morphologies have attracted considerable interest because of their unique properties, such as low density, large surface area, and high guest-loading capacity. Among these hollow nanomaterials, hollow

* Address correspondence to jlshi@sunm.shcnc.ac.cn; ypli@mail.shcnc.ac.cn.

Received for review August 27, 2011 and accepted November 9, 2011.

Published online November 09, 2011
10.1021/nn2033105

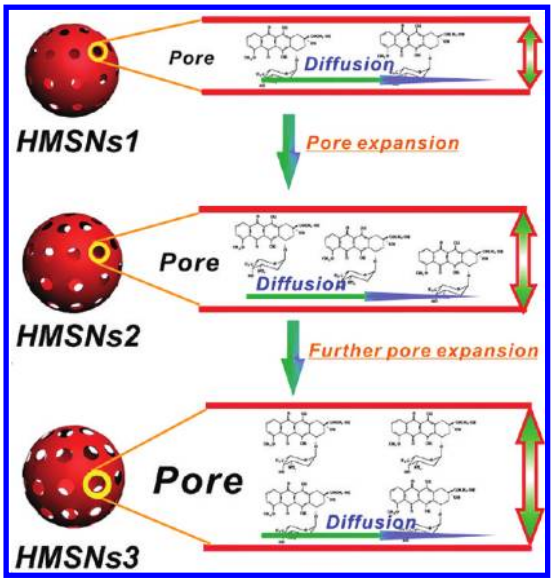

Scheme 1. Representative schematic illustration of controlling doxorubicin release rate by tuning the pore sizes of HMSNs to 3.2 nm (HMSNs1), 6.4 nm (HMSNs2), and 12.6 nm (HMSNs3). It was anticipated that small pores provided limited room for the diffusion of doxorubicin, while large ones could provide enough room for the fast diffusion of drug molecules, which would lead to higher release rate of drug molecules.

mesoporous silica nanoparticles (HMSNs) are of substantial significance in nanobiomedical fields because of their large surface area, high pore volume, tunable pore sizes, and excellent biocompatibility.[13−17] In particular, if the pores in the HMSNs shell were tuned, the nanocarriers could combine the merits of large surface area/high pore volume/hollow interior for efficient drug encapsulation, tunable pore sizes for controlled drug delivery, and hollow interior for reduction of foreign material deposition *in vivo*. Although some important progress of HMSNs in chemotherapy had demonstrated the obvious potential *in vitro* and *in vivo*,[15−17] to the best of our knowledge, there has been no report on HMSNs as DDSs to deliver therapeutic agents against MDR cells with the evaluation of biological effects.

In this work, we employed HMSNs as DDSs to deliver a typical chemotherapeutic agent, doxorubicin (DOX), into drug-resistant cancer cells (MCF-7/ADR) and tuned the pore sizes of HMSNs in the range from 3.2 to 12.6 nm to control the doxorubicin release rate for the first time (Scheme 1). The *in vitro* cytotoxicity, cellular uptake efficiency, intracellular drug release behavior, P-gp expression, and ATP level in MCF-7/ADR cells after treatment with HMSNs or DOX-loaded HMSNs (DMSNs) were extensively evaluated to clarify the biological roles of HMSNs with different pore sizes in the reversion of MDR.

RESULTS

Preparation and Characterization of DMSNs. HMSNs with three different pore sizes of 3.2 nm (HMSNs1), 6.4 nm (HMSNs2), and 12.6 nm (HMSNs3) were successfully synthesized (Figure 1) according to our recently developed selective etching process.[18] Figure 1A shows the schematic illustration of the microstructures of HMSNs, which were composed of a huge hollow cavity in the core part and the nanoporous silica shell. These HMSNs with special hollow structure were synthesized by a structural difference-based selective etching strategy, which utilized the differences of condensation/densification degrees of silica source of solid silica core/mesoporous silica shell ($sSiO_2$@$mSiO_2$) nanoparticles. After the treatment of $sSiO_2$@$mSiO_2$ in Na_2CO_3 aqueous solution, the core part could be selectively etched away to create the hollow structure.

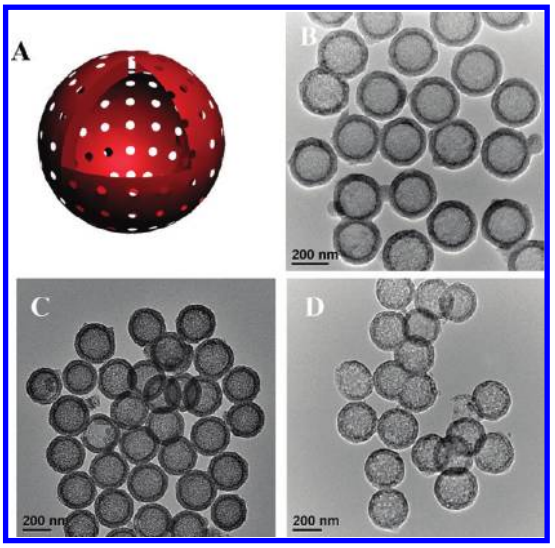

Figure 1. Schematic illustration of HMSNs with hollow interior and nanopores in the shell (A). TEM images of HMSNs1 with a pore size of 3.2 nm (B), HMSNs2 with a pore size of 6.4 nm (C), and HMSNs3 with a pore size of 12.6 nm (D).

As shown in Figure 1B, HMSNs exhibited a highly uniform and monodispersed spherical morphology with a distinctive hollow nanostructure, and the pores in the mesoporous silica shell were randomly distributed. The pores in the shell could be enlarged by adopting varied etching time. The successful fabrication of large-pore-sized HMSNs was demonstrated by transmission electron microscopy (TEM) (Figure 1C, D), which showed that the white dots representing the pores became larger with a longer etching time.

To evaluate their capacity as release-controlled drug delivery vehicles, DOX was selected and loaded into three HMSNs to prepare DOX-loaded HMSNs. The loading efficienty of DOX in HMSNs was 59.6% (HMSNs1), 50.1% (HMSNs2), and 65.1% (HMSNs3), respectively. HMSNs showed high loading capacity, which could be because of the high surface-to-volume ratio and the electrostatic interaction between positively charged DOX molecules and the negatively charged silica nanoparticles.

***In Vitro* Release Behavior of DMSNs.** The *in vitro* release of DOX from DMSNs with three pore sizes was

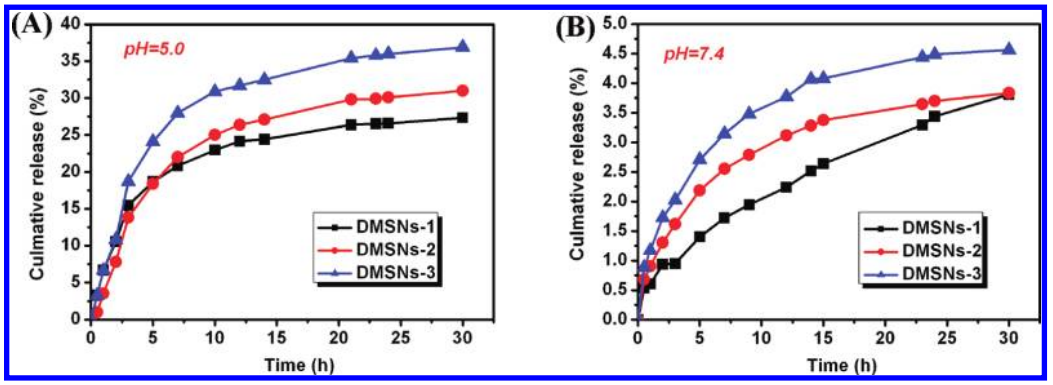

Figure 2. *In vitro* **drug release of DMSNs in different PBS with pH 5.0 (A) and pH 7.4 (B).**

examined in different phosphate-buffered solutions (PBS). Figure 2 shows that DMSNs could release DOX in a controlled release manner, and the drug release rate was dependent on the pore size of HMSNs in PBS with the same pH. In two pH conditions, DMSNs with larger pore size showed faster drug release rate. DMSNs also demonstrated a pH-responsive drug release character. In PBS (pH 7.4) to simulate normal physiological conditions, only a very small amount of DOX was released from DMSNs in a very slow fashion; indeed in DMSNs3, the cumulative release of DOX was only about 4.5% within 30 h. However, in PBS at pH 5.0 to simulate the intracellular conditions of cancer cells, the release rate of DOX from DMSNs became much faster. The cumulative release of DOX from DMSNs3 could reach as high as about 35% within 30 h. Even if in PBS at pH 6.0, the cumulative release of DOX from DMSNs1 with the smallest pore size also could reach about 25% within 24 h (Figure S1).

***In Vitro* Cytotoxicity and Cellular Uptake of HMSNs.** The cytotoxicity of HMSNs was first measured in both MCF-7 and MCF-7/ADR cells. All HMSNs with three pore sizes showed no obvious cytotoxicity at the concentrations of 10 to 100 μg/mL even after culturing for 72 h (Figure 3A, B), which demonstrated the excellent biocompatibility of HMSNs.

The cellular uptake of HMSNs in MCF-7 and MCF-7/ADR cells was investigated using green-emitting fluorescent dye, fluorescein isothiocyanate (FITC), labeled HMSNs (FMSNs) by flow cytometry (FCM). All three HMSNs could efficiently enter cancer cells within 2 h of incubation (Figure 3C, D). HMSNs with larger pore size showed higher cellular uptake efficiency, which could be attributed to the following reasons: on one hand, for nanoparticles with the same volume, the weight of nanoparticles with larger pores could be lighter than that of nanoparticles with smaller pores, and for nanoparticles of the same concentration, the number of HMSNs with larger pores could be more than that of HMSNs with smaller pores. The greater the number, the greater the chance that the nanoparticles were taken up. One the other hand, some fluorophores passively encapsulated inside the hollow volume of nanoparticles could leak out and enter the cell, and this leakage would be faster in nanoparticles with larger pores. The uptake of HMSNs all showed concentration-dependence. Compared with MCF-7, HMSNs were more likely to be taken up by drug-resistant MCF-7/ADR cells. The mean fluorescent intensity could reach as high as 4544.97 in MCF-7/ADR cells after being incubated with 20 μg/mL FMSNs3, while the mean fluorescent intensity was only 1987.11 in MCF-7 cells. From these results, it could be concluded that HMSNs showed promising potential as a delivery system for chemotherapeutic drugs, especially for delivering chemotherapeutic drugs into drug-resistant cancer cells.

The cellular uptake of FMSNs was also observed qualitatively by confocal laser scanning microscopy (CLSM) with the nucleus and lysosome stained by Hoechst 33342 and LysoTraker Red, respectively. The green fluorescence could distribute inside the cells, which indicated that all three FMSNs could be taken up by MCF-7/ADR cells. Much of the green fluorescence was around the membrane in cells treated with FMSNs1 and FMSNs2, while the co-localization of green and red fluorescence could be easily observed in cells treated with FMSNs3, which indicated the most efficient cellular uptake of FMSNs3 (Figure 3E, F, G), which was consistent with the above qualitative results.

Cellular Uptake of DMSNs. To confirm that the efficient uptake of DMSNs by cancer cells could facilitate cellular uptake of DOX loaded into HMSNs, the cellular uptake of DOX in both MCF-7 and MCF-7/ADR cells was measured quantitatively by FCM (Figure 4). Compared with free DOX, DMSNs did not show increased uptake in drug-sensitive MCF-7 cells except DMSNs with 5 μg/mL DOX concentration (Figure 4A). However, significantly improved uptake efficiency was found in MCF-7/ADR cells after treatment with DMSNs compared with free DOX. The uptake efficiency of DMSNs was closely related to the pore size of DMSNs, and the best uptake efficiency was obtained in the DMSNs3-treated group with the largest pore size (Figure 4B), which was consistent with the previous uptake results that HMSNs with larger pore size showed higher cellular uptake efficiency.

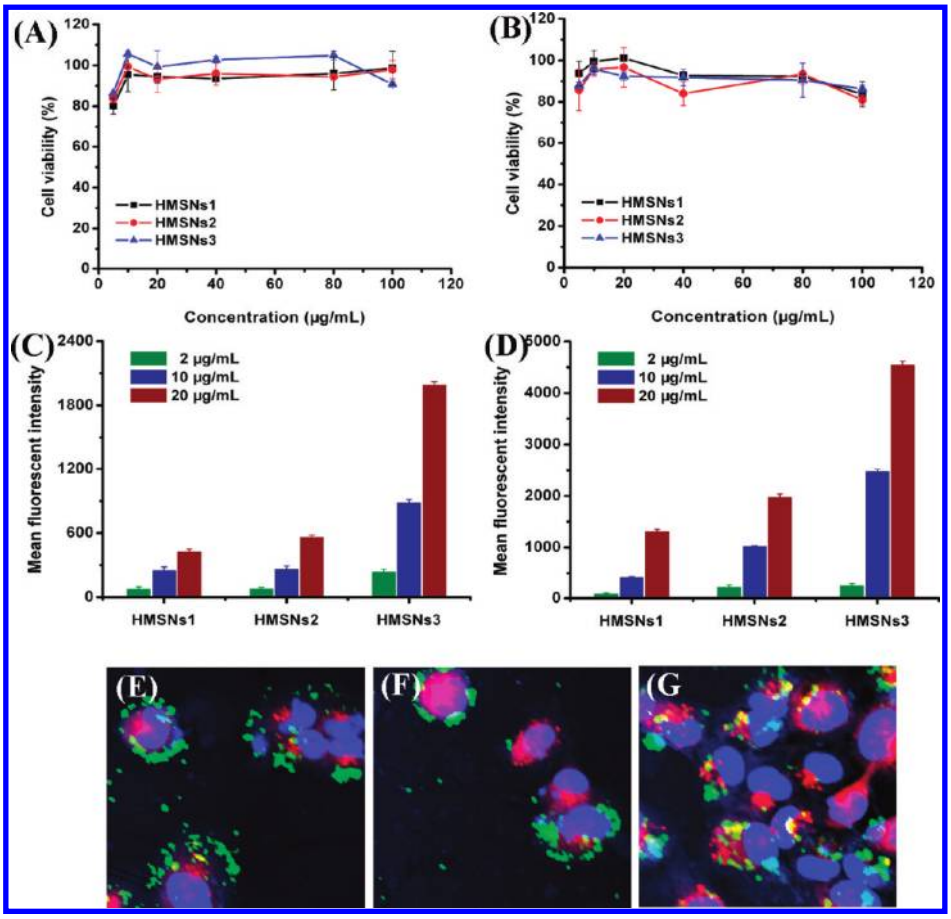

Figure 3. *In vitro* **cytotoxicity and cellular uptake of HMSNs with different pore sizes against MCF-7 and MCF-7/ADR cells. Cytotoxicity of HMSNs against MCF-7 (A) and MCF-7/ADR cells (B) at a concentrations of 10 to 100 μg/mL after 72 h incubation time. Cellular uptake of HMSNs labeled with FITC at different concentrations after 2 h incubation in MCF-7 (C) and MCF-7/ADR cells (D). Confocal microscopic images of MCF-7/ADR cells after incubating with FITC-labeled HMSNs1 (E), HMSNs2 (F), or HMSNs3 (G) (10 μg/mL, green) for 2 h. The cell nucleus was stained with Hoechst 33342 (blue), and the lysosome stained with LysoTraker Red (red).**

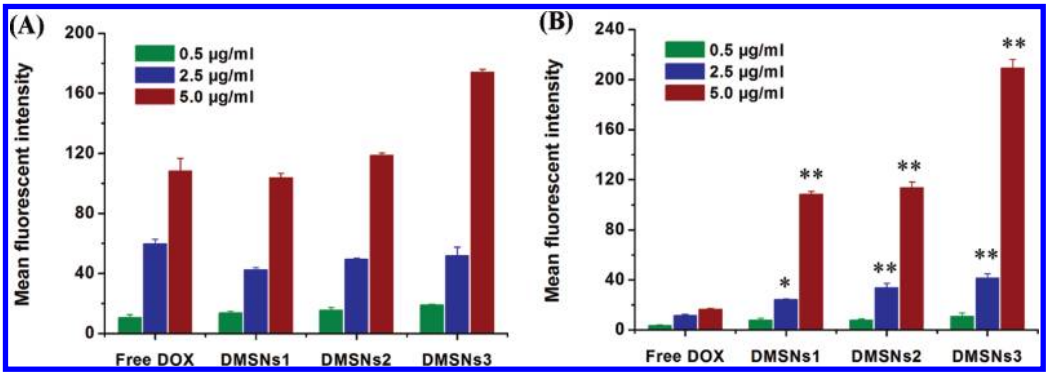

Figure 4. Cellular uptake of DOX loaded in HMSNs with different pore sizes against MCF-7 (A) and MCF-7/ADR (B) cells. Cells were incubated with free DOX or DMSNs for 2 h. *$p < 0.05$ and **$p < 0.01$ compared with free DOX group.

***In Vitro* Cytotoxicity of DMSNs.** To determine whether DMSNs could reverse MDR, the cytotoxicity of DMSNs was evaluated against MCF-7 and MCF-7/ADR cells. In drug-sensitive MCF-7 cells, free DOX and three DMSNs all showed dose-dependent toxicity, and DMSNs demonstrated a little higher toxicity compared with free DOX (Figure 5A). The half-maximal inhibitory concentration (IC_{50}) of free DOX, DMSNs1, DMSNs2, and DMSNs3 against MCF-7 cells after 72 h treatment was 334.9, 245.2, 182.0, and 141.6 ng/mL, respectively. The toxicity did not obviously increase, which could result from the good water solubility of DOX and the efficient cellular uptake of free DOX by drug-sensitive cells.

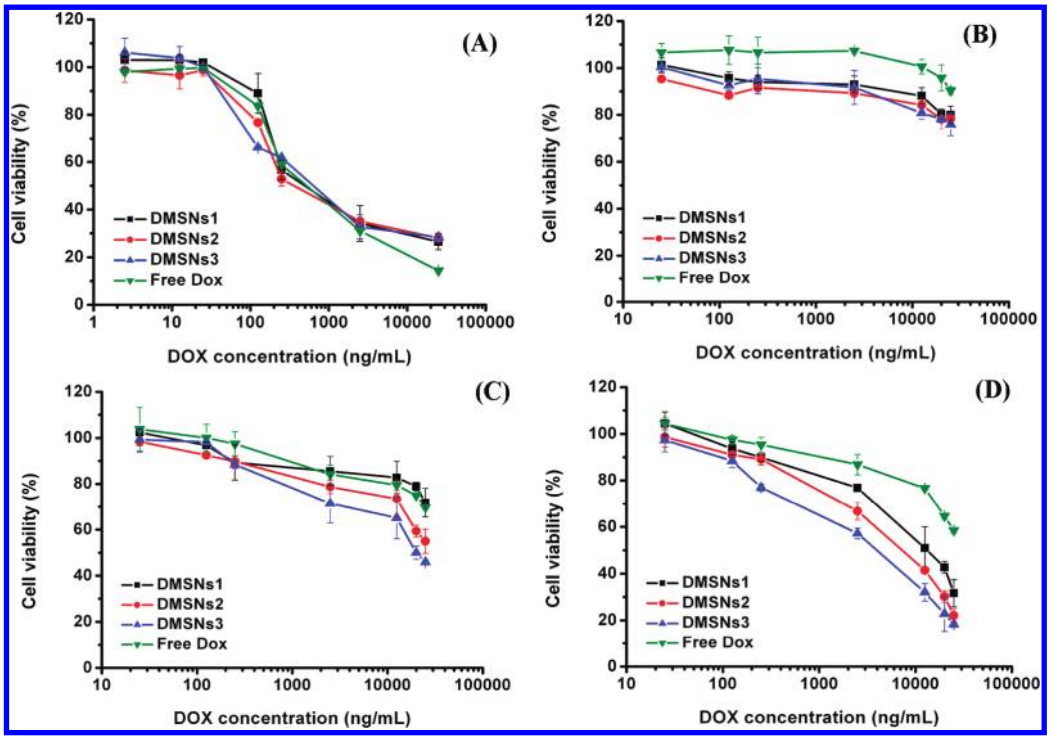

Figure 5. *In vitro* **cytotoxicity of DMSNs with different pore sizes against MCF-7 and MCF-7/ADR cells. (A) Cell viability of MCF-7 cells after incubating with DMSNs at different concentrations for 72 h. Cell viability of MCF-7/ADR cells after incubating with DMSNs at different concentrations for 24 h (B), 48 h (C), and 72 h (D).**

As for drug-resistant MCF-7/ADR cells, free DOX did not exhibit visible cytotoxicity from 24 to 48 h due to the overexpression of P-gp on the cell membrane of MCF-7/ADR to pump the drug out.[17] The toxicity of free DOX occurred only when the incubation was extended to 72 h (Figure 5B, C, D), and the cell viability was still over 50% after treatment with 25 μg/mL DOX, which proved the strong resistance of MCF-7/ADR cells to DOX. Compared with free DOX, DMSNs showed remarkable cytotoxicity, and the cytotoxicity was dependent on the treatment time. The IC_{50}'s of DMSNs1, DMSNs2, and DMSNs3 against MCF-7/ADR cells after 72 h treatment were 8.7, 5.7, and 3.5 μg/mL, respectively (Figure 5D). These results suggested that DMSNs could facilitate the cellular uptake of drug into MCF-7/ADR cells to overcome DOX resistance. In addition, it was found that the toxicity of DMSNs against MCF-7 and MCF-7/ADR cells was related to pore size. The IC_{50} value of DMSNs decreased with an increase in pore size of the HMSNs. This could be due to the pore-size-dependent cellular uptake of HMSNs, which had been proved by quantitatively measuring the cellular uptake as mentioned above. Furthermore, the toxicity of DMSNs was related to incubation time in MCF-7/ADR cells, and DMSNs with larger pore size exhibited more obvious time-dependence. When the incubation time increased to 48 h, the three DMSNs showed different toxicity, and DMSNs with the largest pore size showed the maximum toxicity. When the incubation time increased further, the trend became more evident. Apart from the different cellular uptake efficiency of DMSNs in MCF-7/ADR cells, the different release rate of DOX from HMSNs with different pore sizes could be another reason, which was proved as mentioned below.

DOX could exert cytotoxic effects through cell cycle arrest.[19] To evaluate the mechanism of cytotoxic effects of DMSNs, the cell cycle progression of MCF-7/ADR cells after treatment with DMSNs was assessed by analysis of DNA content using FCM. As shown in Figure 6, after treatment with three HMSNs for 72 h, a little more G1 phase of the cells was observed, which indicated that HMSNs had some effect on cell cycle distribution. Different from HMSNs, DMSNs could induce cell cycle arrest at the G2/M phase, which demonstrated a similar mechanism to free DOX. All DMSNs showed superior effects on cell cycle arrest to free DOX, and DMSNs with a larger pore size demonstrated enhanced cell cycle arrest, which was consistent with the *in vitro* cytotoxicity results.

Intracellular Drug Release Behavior of DMSNs. According to the *in vitro* release profile of DMSNs (Figure 2), it could be found that DMSNs showed a pH-responsive drug release, and the drug release rate increased with an increase in pore size. As a result, after efficient uptake into cancer cells, DOX could be released from DMSNs to exert its function. The intracellular DOX release processes of three DMSNs in MCF-7 and MCF-7/ADR cells showed that the intracellular DOX concentration increased with in increased incubation time (Figure 7), which indicated that DOX could be sustainedly

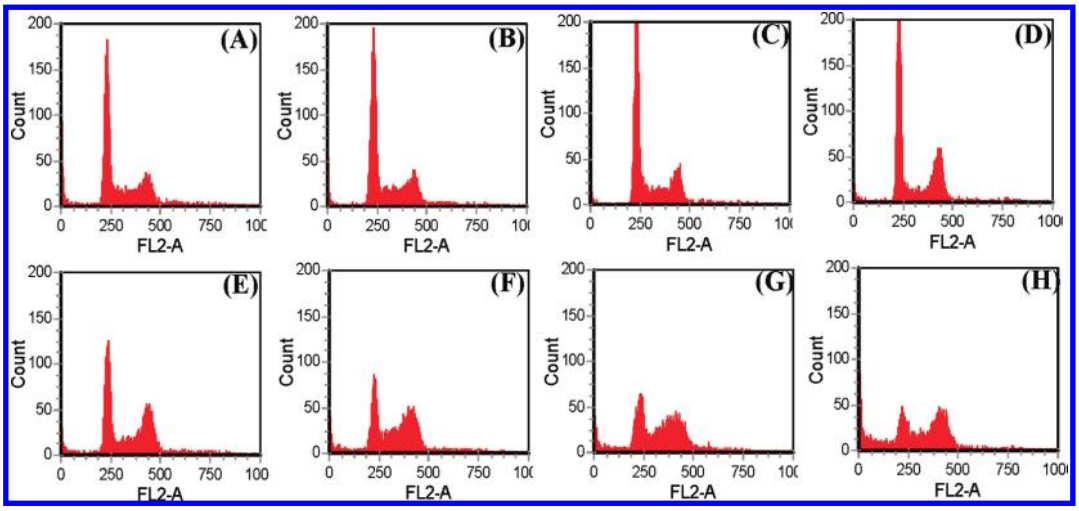

Figure 6. Effects of treatment with HMSNs, free DOX, or DMSNs for 72 h on the cell cycle of MCF-7/ADR cells. Control cells (A); cells treated with HMSNs1 (B), HMSNs2 (C), or HMSNs3 (D) at 40 μg/mL; cells treated with free DOX at 10 μg/mL (E); cells treated with DMSNs1 (F), DMSNs2 (G), or DMSNs3 (H) at an equivalent DOX concentration of 10 μg/mL.

released from DMSNs. In MCF-7/ADR cells, the intracellular free DOX reduced in some time points before 12 h, which could result from P-gp-mediated drug efflux (Figure 7B). When the incubation time was extended, the release of DOX from DMSNs increased, and in the meantime, the drug efflux decreased because of the reduction of P-gp expression and ATP level in MCF-7/ADR cells by the action of HMSNs, which was proved as mentioned below. According to the release curves, it is very obvious that the intracellular DOX concentration was higher in MCF-7/ADR cells than in MCF-7 cells, and the cells treated with DMSNs with larger pore size showed a higher intracellular released DOX concentration. In addition, the intracellular DOX distribution from a confocal microscope at 24, 48, and 72 h showed that both the released DOX and nonreleased DOX (the red particles) were almost distributed in the cytoplasm within 24 h (Figure 7C), while the assembly of DOX to the nucleus could be found after 48 h, which suggested that an efficient cellular uptake of DMSNs and the gradual release of DOX from DMSNs occurred.

Determination of P-gp Expression and the ATP Level in MDR Cells. The measurement of the expression of P-gp in tumor cells is an important aspect in analyzing the reversal of drug resistance. In our other work, we found that P-gp was overexpressed on the membrane of MCF-7/ADR cells, and this is closely related to its drug resistance property.[20] To evaluate the effects of HMSNs on P-gp function of drug-resistant cells, MCF-7/ADR cells were incubated with different concentrations of HMSNs for 24 and 48 h (Figure 8A, B). The inhibition of P-gp expression due to HMSNs was dose-dependent after 48 h and not related to pore size. The obvious reduction of P-gp expression by HMSNs3 could be due to the efficient cellular uptake and high concentration of HMSNs3 in MCF-7/ADR cells exerting strong effects on P-gp expression.

HMSNs also showed slight inhibition effects on the cellular ATP level (Figure 8C, D). HMSNs1 in high concentration demonstrated the strongest inhibition on ATP at both 24 and 48 h. The ATP levels all decreased after treatment with three HMSNs at 48 h, and cells treated with a high concentration of HMSNs showed a low level of ATP, which indicated that HMSNs could decrease drug efflux through a decrease inenergy provision.

DISCUSSION

During the last few decades, the development of drugs for cancer therapy has focused on new DDSs to deliver drugs in a site-, dose-, and time-correct manner.[21,22] Because the development of cancer or MDR cancer is a multistep process involving the interaction between genes and their environment, the appropriate dose selection and exposure time arrangement could be two significant factors in enhancing efficacy and improving patient compliance. On one hand, a prolonged therapeutic level of drugs could be maintained by sustained drug release, and the frequency of dosing can be consequently reduced.[23,24] On the other hand, a specific drug has a specific mechanism of action, and control of the cellular retention of drug and its time of action are needed.[9]

The development of advanced controlled drug delivery systems requires careful selection of components and configurations. Nowadays, the release of drugs from organic DDSs can be achieved by diffusion-controlled systems, swelling-controlled systems, and erosion-controlled systems.[25] Inorganic DDSs also could be used as controlled drug release systems by chemical modification of the particle surface by organic functionalization.[26,27] Among the inorganic nanoparticles, the porous ones especially possess the advantages of high stability and tunable pore size to

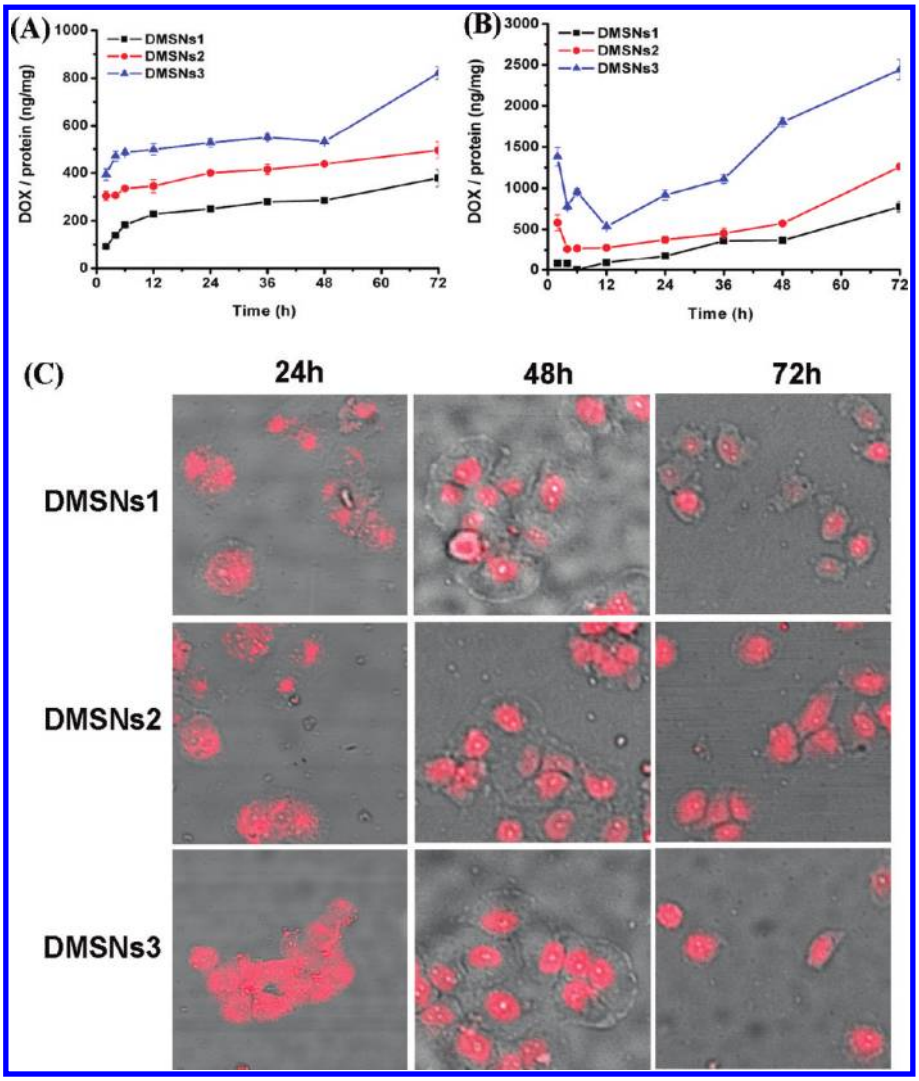

Figure 7. Quantitative and qualitative evaluation of intracellular DOX release from DMSNs with different pore sizes. Quantitative measurement of intracellular drug release behavior of DMSNs in MCF-7 (A) and MCF-7/ADR cells (B). Qualitative observation of intracellular DOX release from DMSNs with different pore sizes at representative treatment time periods in MCF-7/ADR cells (C).

control drug release. However, it is still a big challenge to elaborately design these drug carriers with an accurate drug release rate. Mesoporous silica nanoparticles with different pore sizes have been reported to control the release of the water-soluble drug captopril, but the pore size of MSNs was controlled by using different kinds of surfactants, and the composition, microstructure, nanoparticle size, and sphere morphology were all different among the MSNs.[28] The HMSNs that we developed here were based on structural differences rather than traditional compositional differences with tailored pore sizes, similar composition, and morphology. Our experimental result demonstrated that the pore size of HMSNs could be tuned to precisely control the drug release rate for the first time. From the results of the *in vitro* release (Figure2, Figure S1) and intracellular drug release (Figure 7), it could be easily found that the drug release rate in the same pH conditions was closely related to the pore size. The control of the release rate from HMSNs could be based on the confinement effect of mesoporous channels and the diffusion rate of the drug from the pores.

Besides the pore-size-controlled release character, DMSNs also demonstrated a pH-responsive drug release. Endowing DDSs with pH-responsive drug release character has been proved to be an effective way to enhance drug efficacy and reduce toxicity.[29,30] Ideal DDSs would responsively release drug only at the tumor site and not in normal tissue. The pH-responsive drug release mechanism for DMSNs should be due to the electrostatic attraction between HMSNs and DOX.[31−33] The positively charged DOX within HMSNs could exchange with protons in acidic conditions, but was not exchangeable in pH = 7.4 release media. This pH-responsive and sustained drug release could favor increased intracellular DOX accumulation and reduced DOX efflux and, thus, was useful to enhance the long-term anticancer efficacy.

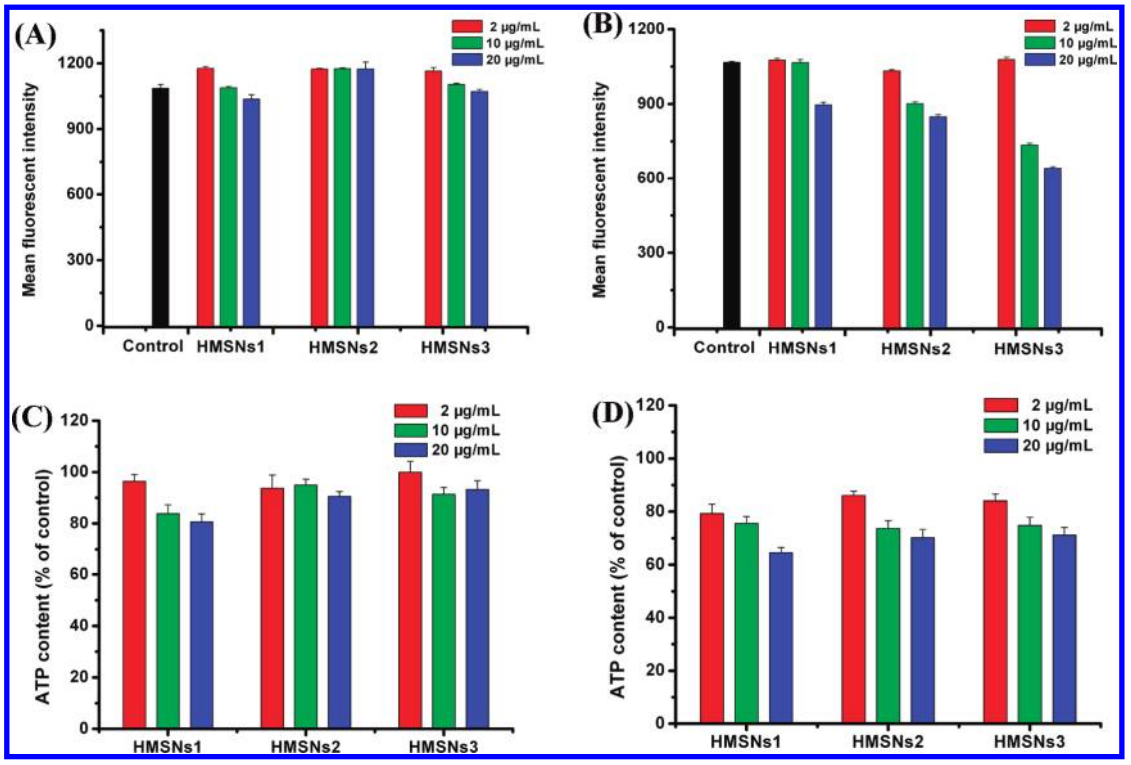

Figure 8. Determination of P-gp expression and ATP level in MCF-7/ADR cells. P-gp expression on the MCF-7/ADR cell membrane after treatment with different HMSNs for 24 h (A) or 48 h (B). ATP depletion in MCF-7/ADR cells after treatment with different HMSNs for 24 h (C) or 48 h (D).

To our knowledge, this is also the first report on using HMSNs as DDSs to deliver a chemotherapeutic agent into drug-resistant cancer cells to overcome MDR. So far, some inorganic nanoparticles including gold,[34] Fe_3O_4,[35] and carbon nanotubes,[36] have been used as carriers to overcome MDR; however, further functionalizing them with desirable controllable release of drug seems to be a problem. To investigate whether HMSNs could be used as drug delivery systems to reverse MDR, the toxicity and cellular uptake in both MCF-7 and MCF-7/ADR cells were examined first. HMSNs showed negligible toxicity in both MCF-7 and MCF-7/ADR cells (Figure 3) and demonstrated superior cellular uptake efficiency in drug-resistant MCF-7/ADR cells to drug-sensitive MCF-7 cells. These exciting phenomena indicated the promising potential of HMSNs to act as delivery systems to overcome MDR for cancer chemotherapy. The superior uptake ability of HMSNs in MCF-7/ADR cells could facilitate more DOX uptake (Figure 4) and intracellular DOX concentration (Figure 7) in MCF-7/ADR cells than in MCF-7 cells. To demonstrate the effects of DMSNs overcoming MDR further, an *in vitro* antiproliferation assay was carried out. From the cytotoxicity results, efficient reversion of MDR could be found after treatment with DMSNs. The longer the incubation time, the higher the cytotoxicity to MDR cancer cells (Figure 5). This could be attributed to the following reasons: (1) the efficient cellular uptake of DOX loaded in DMSNs. The results from both FCM and CLSM demonstrated that DOX carried by HMSNs could be efficiently delivered into MDR cancer cells. (2) The pH-responsive release manner of DMSNs could maximumly reduce drug degradation outside the cells and increase drug concentration inside the cancer cells. (3) The sustained intracellular release ability of DOX from DMSNs could reduce drug efflux by P-gp because the free DOX rather than the nanoparticle was the substrate of P-gp. (4) The inhibition effects of HMSNs on P-gp expression and ATP level could further suppress drug efflux, which led to increased intracellular drug concentration and enhanced cytotoxicity. As the P-gp transporter could utilize energy from ATP hydrolysis to transport anticancer drugs[37] and overexpression of P-gp on the membrane of the MCF-7/ADR cell line is one of the most crucial mechanisms of its drug-resistant property,[20] inhibition of P-gp and ATP could significantly reverse MDR in MCF-7/ADR cells. (5) Efficient cell cycle arrest is shown by DOX released from DMNSs. In this work, DOX was physically absorbed to HMSNs due to electronic and hydrophobic interactions; therefore, the avoidance of chemical ligation would maximally preserve the molecular integrity of DOX to exert its anticancer activity.

Moreover, the role of pore sizes in the biological effect of HMSNs toward drug-resistant cancer cells was evaluated. Figure 3 shows that the cellular uptake efficiency increases with increasing pore size, which suggested that the physicochemical properties of HMSNs showed significant impacts on their cellular

uptake efficiency. From the results of *in vitro* cytotoxicity, pore-size-dependent toxicity was found in both MCF-7 and MCF-7/ADR cells. DMSNs with larger pore size could suppress cancer cells more effectively, which could be due to the more efficient cellular uptake (Figure 4) and higher intracellular drug concentration through faster release of DOX from DMSNs (Figure 7) with larger pore size. These results indicated that the pore sizes of DMSNs had great effects on anticancer effects against drug-resistant cancer cells, which implied that the biological effects of HMSNs could be regulated by pore size to meet clinical needs.

CONCLUSIONS

In this work, HMSNs with three pore sizes were manufactured to control the drug release rate, and the biological roles of these HMSNs were evaluated in multidrug-resistant cancer cells. DMSNs exhibited pore-size-dependent, high anticancer activity against MCF-7/ADR cells. The MDR-overcoming mechanism could be due to efficient cellular uptake, P-gp inhibition, and ATP depletion. These results demonstrated that HMSNs could be very promising drug delivery systems for pore-size-controllable drug release and cancer MDR reversion.

EXPERIMENTAL SECTION

Materials. Doxorubicin (DOX, purity >99%) was purchased from Zhejiang Hisun Pharmaceutical Co., Ltd. (Zhejiang, China). Trypsin-EDTA and phosphate-buffered saline (PBS) were obtained from Gibco-BRL (Burlington, ON, Canada). The RPMI 1640 medium, antibiotics, and fetal bovine serum (FBS) were purchased from Invitrogen GmbH (Karlsruhe, Germany). Hoechst 33342 was purchased from Molecular Probes (Eugene, OR, USA). 3-(4,5-Dimethylthiazol-2-yl)-2,5-diphenyltetrazolium bromide (MTT), DNA-free RNase A, and propidium iodide (PI) were purchased from Sigma (St. Louis, MO, USA). Coumassie brilliant blue G250 for the Bradford protein assay and tetraethyl orthosilicate (TEOS) were purchased from Sinopharm Chemical Reagent Co., Ltd. (Shanghai, China). Octadecyltrimethoxysilane (C_{18}TMS) was purchased from Tokyo Chemical Industry Co., Ltd. (Japan). The ATP assay kit was purchased from Beyotime Institute of Biotechnology (Shanghai, China). Phycoerythrin (PE)-anti-human MDR1 (CD243, P-gp, ABCB1) and PE-mouse IgG2a (κ Isotype Control) were obtained from eBioscience (CA, USA). Cell lysis buffer was purchased from Promega Corporation (Madison, WI, USA). All other chemicals and solvents if not mentioned were of analytical grade and used as received without additional purification.

Cell Lines and Cell Culture. Drug-sensitive human breast cancer cell line MCF-7 and its DOX-resistant counterpart MCF-7/ADR cell line were purchased from Nanjing KeyGen Biotech. Co., Ltd. (China). Cells were cultured in RPMI-1640 medium supplemented with 10% FBS, 100 U/mL penicillin G sodium, and 100 μg/mL streptomycin sulfate and maintained at 37 °C in a humidified and 5% CO_2 incubator. To maintain the resistant phenotype, MCF-7/ADR cells were maintained in the medium containing 1 μg/mL DOX and were cultured in drug-free medium for 48 h before the experiments.

Preparation and Characteristics of DOX-Loaded HMSNs. The synthesis of HMSNs with three different pore sizes was performed as described in our previous work with some minor modification, and the pore sizes of HMSNs were measured by the typical N_2 absorption−desorption technique.[18,38] Briefly, ethanol (71.4 mL), H_2O (10 mL), and ammonium solution (3.14 mL) were mixed and stirred at 30 °C. Then, TEOS (6 mL) was added into the mixture, and the reaction lasted for another 1 h. TEOS (5 mL) and C_{18}TMS (3 mL) were premixed and added into the reaction medium rapidly afterward, and the reaction lasted for another 1 h. Finally, the obtained nanoparticles were dispersed into Na_2CO_3 aqueous solution (0.6 M) for different etching times (0.5, 4, and 7 h) at 80 °C. The product was collected by centrifugation and washed with water thoroughly. The C_{18}TMS was removed by calcination at 550 °C for 6 h. For the preparation of DMSNs, 5 mg of HMSNs with different pore sizes was dispersed into DOX aqueous solution (0.5 mg/mL, 6 mL). After dispersion and stirring under light-sealed conditions for 12 h, DMSNs were obtained by centrifugation and washed with 20 mL of PBS (pH 7.4), then dried under vacuum at room temperature. TEM images were acquired on a JEM-2100F electron microscope operating at an accelerating voltage of 200 kV. To evaluate the DOX loading efficiency, the supernatant was collected, and the residual DOX content (R_{DOX}, mg) was determined using the calibration curve of DOX standard solutions by the UV−vis measurement at 495 nm. The loading efficiency of DOX in HMSNs was calculated as follows:

$$\frac{\text{initialamountofDOX} - \text{residualDOX}}{\text{initialamountofDOX}} \times 100\%$$

***In Vitro* Drug Release of DMSNs in PBS with Different pH Values.** To measure *in vitro* drug release, 8 mg of DMSNs including HMSNs1, HMSNs2, or HMSNs3 was put into a pretreated dialysis bag with 1/3 air gap and sealed with a dialysis bag holder, respectively. The sealed dialysis bag was put into the brown bottle with 18 mL of PBS (pH = 5.0 or 7.4). The bottle was shaken at 100 rpm at 37 °C under light-sealed conditions. At certain time intervals, 3 mL of the release medium was taken out to measure the released drug concentration and then was returned to the original release medium. For the measurement of released DOX concentration, the absorbance of the release medium at 495 nm was recorded on a Shimadzu UV-3101PC UV−vis absorption spectrophotometer.

***In Vitro* Antiproliferation Assay.** The cytotoxicity of DMSNs with different pore sizes was evaluated by the MTT method. MCF-7 and MCF-7/ADR cells were seeded at a density of 8000 cells/well in 96-well plates and grown for 24 h. The growth media were replaced by fresh complete medium containing blank HMSNs, free drug, or DMSNs with different concentrations and incubated for different times. After different time intervals, cells were incubated with MTT working solution (final concentration of 0.5 mg/mL) at 37 °C for 4 h. The dark blue formazan crystals formed were dissolved with DMSO. The absorbance was measured at a wavelength of 570 nm using an automated plate reader (Tecan Spectrafluor Plus, Austria). All drug concentrations were tested in six replicates.

Cellular Uptake Experiment. In order to track the cellular uptake of HMSNs, HMSNs were labeled with FITC. First, 15 mg of FITC was reacted with 3-aminopropyltriethoxysilane (APTES, 100 μL) in 5 mL of ethanol solution under dark conditions for 24 h. Then, 20 mg of HMSNs was reacted with FITC-APTES stock solution (1 mL) in the dark for 24 h. The FMSNs were collected by centrifugation and washed with ethanol several times. Finally, FMSNs were dried under vacuum at room temperature.

The cellular uptake ability of FMSNs and DMSNs was measured by FCM. MCF-7 and MCF-7/ADR cells were seeded in a 24-well plate at a concentration of 1×10^5 cells/well and allowed to attach for 24 h. Then, the growth medium was removed, and cells were incubated with FMSNs at 2, 10, and 20 μg/mL or incubated with free DOX or DMSNs at a DOX concentration of 0.5, 2.5, or 5 μg/mL for 2 h at 37 °C. After that, the cells were washed three times with PBS (pH 7.4), then trypsinized and centrifuged at 2000 rpm. The cell resuspension

was finally subjected to FACScan flow cytometry (Beckton Dickinson, USA) and analyzed with CellQuest software through fluorescence channel 1 (FL1) for FMSNs or fluorescence channel 2 (FL2) for DOX.

For confocal observation, MCF-7/ADR cells were seeded on 10 mm^2 glass coverslips in 24-well plates at a density of approximately 1×10^5 cells per well in 500 μL of growth medium and allowed to attach for 24 h. After incubation with FMSNs for 2 h at 37 °C, the medium was removed, and the cells were washed three times with PBS. The intracellular distribution of FMSNs was observed by CLSM after staining lysosomes with LysoTracker Red (Molecular Probes, Eugene, OR, USA) and nuclei with Hoechst 33342 (Sigma, USA). The CLSM observation was performed using a FLuoView FV1000 confocal microscope (Olympus Microsystems, Japan) with a 40× objective at excitation wavelengths of 633 nm (He−Ne laser), 488 nm (Ar laser), and 351 nm (UV laser) for LysoTrakcer Red (red), FMSNs (green), and Hoechst 33342 (blue), respectively.

Intracellular DOX Release and Confocal Microscopic Observation. Release of DOX from MCF-7 or MCF-7/ADR cells was examined by detecting the fluorescence of the released DOX in the cell medium. MCF-7 and MCF-7/ADR cells were exposed to DMSNs at a DOX concentration of 2.5 μg/mL. After various time points, the cells were washed three times with PBS (pH 7.4), then lysed for 2 min in lysis buffer and centrifuged at 4000 rpm. The supernatants were collected, and the fluorescence of the released DOX was measured using an automated plate reader (Tecan Spectrafluor Plus, Austria) at 480 nm excitation and 595 nm emission wavelengths. Supernatants from equal numbers of cells corresponding to equal amounts of protein were determined by the Bradford protein assay.

For confocal observation, MCF-7/ADR cells were seeded on 10 mm^2 glass coverslips in 24-well plates at a density of approximately 1×10^5 cells per well in 500 μL of growth medium and allowed to attach for 24 h. Cells were incubated with DMSNs at a DOX concentration of 2.5 μg/mL at 37 °C for 24, 48, and 72 h. After incubation, the coverslips were taken out, rinsed three times at 37 °C using preheated PBS, fixed with 4% paraformaldehyde, and observed by CLSM.

Detection of P-gp Expression and ATP. The cell surface P-gp levels were measured by FCM. MCF-7/ADR cells were seeded into 24-well plates at a density of 1×10^5 cells/well and cultured for 24 h. The media was replaced with fresh growth medium containing HMSNs at 2, 10, or 20 μg/mL for 24 or 48 h. Then the cells were trypsinized, collected, and resuspended in PBS (pH 7.4). PE-conjugated mouse anti-human monoclonal antibody against P-gp was used to label cells according to the manufacturer's instruction, and the nonspecific labeling was corrected by its isotype control. The fluorescent intensity was determined by FCM and analyzed with CellQuest software through FL2.

For determination of ATP, MCF-7/ADR cells were seeded in 24-well plates at a density of 1×10^5/well and incubated overnight. Following treatment with three HMSNs without loading DOX at 2, 10, or 20 μg/mL for 24 or 48 h, cells were washed three times with ice-cold PBS and lysed with ATP lysis buffer. The intracellular ATP levels were determined using a luciferine/luciferase assay following the protocol of the ATP assay kit (Beyotime, China). The ATP in the cell lysate was measured using a POLARstar OPTIMA microplate reader (BMG Labtech, Germany) by calibration with the ATP standards.

Cell Cycle Analysis. MCF-7/ADR cells were seeded in six-well plates at a density of 5×10^5/well and incubated overnight. After treating with three DMSNs at a DOX concentration of 10 μg/mL for 72 h, cells were trypsinized, collected, and fixed with 70% precooled ethanol at 4 °C for 24 h. Fixed cells were washed twice with ice-cold PBS, incubated with 1 μg/mL RNase A for 20 min at 37 °C, and then stained with 10 μg/mL PI for 30 min in the dark. Stained cells were analyzed on a FACScan flow cytometer, and the percentage of cells in each phase of the cell cycle was evaluated by the ModFit software (Verity Software House, Topsham, ME, USA).

Statistical Analysis. Data were described as the mean ± standard deviations, and statistical analysis was performed using Student's *t* test. The differences were considered significant for p value < 0.05, and $p < 0.01$ was indicative of a very significant difference.

Acknowledgment. The National Basic Research Program of China (2010CB934000, 2009CB930304, and 2012CB932500), the National Natural Science Foundation of China (30925041 and 50823007), the Science and Technology Commission of Shanghai (No. 10430712800), and the Science Foundation for Youth Scholar of State Key Laboratory of High Performance Ceramics and Superfine Microstructures (No. SKL201001) are gratefully acknowledged for financial support.

Supporting Information Available: The *in vitro* DOX release from DOX-HMSNs1 at different pH values. This material is available free of charge *via* the Internet at http://pubs.acs.org.

REFERENCES AND NOTES

1. Gottesman, M. M.; Fojo, T.; Bates, S. E. Multidrug Resistance in Cancer: Role of ATP-Dependent Transporters. *Nat. Rev. Cancer* **2002**, *2*, 48–58.
2. Szakacs, G.; Paterson, J. K.; Ludwig, J. A.; Booth-Genthe, C.; Gottesman, M. M. Targeting Multidrug Resistance in Cancer. *Nat. Rev. Drug Discovery* **2006**, *5*, 219–234.
3. Lake, D. E.; Hudis, C. A. High-Dose Chemotherapy in Breast Cancer. *Drugs* **2004**, *64*, 1851–1860.
4. Ho, E. A.; Piquette-Miller, M. Regulation of Multidrug Resistance by Pro-Inflammatory Cytokines. *Curr. Cancer Drug Targets* **2006**, *6*, 295–311.
5. Krishna, R.; Mayer, L. D. Multidrug Resistance (MDR) in Cancer. Mechanisms, Reversal Using Modulators of MDR and the Role of MDR Modulators in Influencing the Pharmacokinetics of Anticancer Drugs. *Eur. J. Pharm. Sci.* **2000**, *11*, 265–283.
6. Thomas, H.; Coley, H. M. Overcoming Multidrug Resistance in Cancer: an Update on the Clinical Strategy of Inhibiting P-Glycoprotein. *Cancer Control.* **2003**, *10*, 159–65.
7. Kumbar, S. G.; Nair, L. S.; Bhattacharyya, S.; Laurencin, C. T. Polymeric Nanofibers As Novel Carriers for the Delivery of Therapeutic Molecules. *J. Nanosci. Nanotechnol.* **2006**, *6*, 2591–2607.
8. Reddy, L. H.; Dubernet, C.; Mouelhi, S. L.; Marque, P. E.; Desmaele, D.; Couvreur, P. A New Nanomedicine of Gemcitabine Displays Enhanced Anticancer Activity in Sensitive and Resistant Leukemia Types. *J. Controlled Release* **2007**, *124*, 20–27.
9. Dorai, T.; Aggarwal, B. B. Role of Chemopreventive Agents in Cancer Therapy. *Cancer Lett.* **2004**, *215*, 129–140.
10. Yan, Y.; Ochs, C. J.; Such, G. K.; Heath, J. K.; Nice, E. C.; Caruso, F. Bypassing Multidrug Resistance in Cancer Cells with Biodegradable Polymer Capsules. *Adv. Mater.* **2010**, *22*, 5398–5403.
11. Slowing, I. I.; Trewyn, B. G.; Lin, V. S. Mesoporous Silica Nanoparticles for Intracellular Delivery of Membrane-Impermeable Proteins. *J. Am. Chem. Soc.* **2007**, *129*, 8845–8849.
12. Vivero-Escoto, J. L.; Slowing, I. I.; Lin, V. S. Tuning the Cellular Uptake and Cytotoxicity Properties of Oligonucleotide Intercalator-Functionalized Mesoporous Silica Nanoparticles with Human Cervical Cancer Cells HeLa. *Biomaterials* **2010**, *31*, 1325–1333.
13. Chen, Y.; Chen, H. R.; Zhang, S. J.; Chen, F.; Zhang, L. X.; Zhang, J. M.; Zhu, M.; Wu, H. X.; Guo, L. M.; Feng, J. W.; *et al.* Multifunctional Mesoporous Nanoellipsoids for Biological Bimodal Imaging and Magnetically Targeted Delivery of Anticancer Drugs. *Adv. Funct. Mater.* **2011**, *21*, 270–278.
14. Chen, Y.; Chen, H. R.; Zeng, D. P.; Tian, Y. B.; Chen, F.; Feng, J. W.; Shi, J. L. Core/Shell Structured Hollow Mesoporous Nanocapsules: A Potential Platform for Simultaneous Cell Imaging and Anticancer Drug Delivery. *ACS Nano* **2010**, *4*, 6001–6013.
15. Li, L. L.; Tang, F. Q.; Liu, H. Y.; Liu, T. L.; Hao, N. J.; Chen, D.; Teng, X.; He, J. Q. *In Vivo* Delivery of Silica Nanorattle Encapsulated Docetaxel for Liver Cancer Therapy with Low Toxicity and High Efficacy. *ACS Nano* **2010**, *4*, 6874–6882.

16. Liu, T. L.; Li, L. L.; Teng, X.; Huang, X. L.; Liu, H. Y.; Chen, D.; Ren, J.; He, J. Q.; Tang, F. Q. Single and Repeated Dose Toxicity of Mesoporous Hollow Silica Nanoparticles in Intravenously Exposed Mice. *Biomaterials* **2011**, *32*, 1657–1668.
17. Wang, T. T.; Chai, F.; Fu, Q.; Zhang, L. Y.; Liu, H. Y.; Li, L.; Liao, Y.; Su, Z. M.; Wang, C. A.; Duan, B. Y.; *et al*. Uniform Hollow Mesoporous Silica Nanocages for Drug Delivery *in Vitro* and *in Vivo* for Liver Cancer Therapy. *J. Mater. Chem*. **2011**, *21*, 5299–5306.
18. Chen, Y.; Chu, C.; Zhou, Y.; Ru, Y.; Chen, H.; Chen, F.; He, Q.; Zhang, Y.; Zhang, L.; Shi, J. Reversible Pore-Structure Evolution in Hollow Silica Nanocapsules: Large Pores for siRNA Delivery and Nanoparticle Collecting. *Small* **2011**, *7*, 2935–2944.
19. Kim, H. S.; Lee, Y. S.; Kim, D. K. Doxorubicin Exerts Cytotoxic Effects Through Cell Cycle Arrest and Fas-Mediated Cell Death. *Pharmacology* **2009**, *84*, 300–309.
20. Gao, Y.; Chen, L.; Zhang, Z.; Chen, Y.; Li, Y. Reversal of Multidrug Resistance by Reduction-Sensitive Linear Cationic Click Polymer/iMDR1-pDNA Complex Nanoparticles. *Biomaterials* **2011**, *32*, 1738–1747.
21. Balmayor, E. R.; Azevedo, H. S.; Reis, R. L. Controlled Delivery Systems: from Pharmaceuticals to Cells and Genes. *Pharm. Res.* **2011**, *28*, 1241–1258.
22. Lebret, V.; Raehm, L.; Durand, J. O.; Smaïhi, M.; Werts, M. H.; Blanchard-Desce, M.; Méthy-Gonnod, D.; Dubernet, C. Folic Acid-Targeted Mesoporous Silica Nanoparticles for Two-Photon Fluorescence. *J. Biomed. Nanotechnol.* **2010**, *6*, 176–180.
23. Harper, E.; Dang, W.; Lapidus, R. G.; Garver, R. I., Jr. Enhanced Efficacy of a Novel Controlled Release Paclitaxel Formulation (PACLIMER Delivery System) for Local-Regional Therapy of Lung Cancer Tumor Nodules in Mice. *Clin. Cancer Res.* **1999**, *5*, 4242–4248.
24. Acharya, S.; Sahoo, S. K. PLGA Nanoparticles Containing Various Anticancer Agents and Tumour Delivery by EPR Effect. *Adv. Drug Delivery Rev.* **2011**, *63*, 170–183.
25. Kanjickal, D. G.; Lopina, S. T. Modeling of Drug Release from Polymeric Delivery Systems—A Review. *Crit. Rev. Ther. Drug Carrier Syst.* **2004**, *21*, 345–386.
26. Singh, K. P.; Panwar, P.; Kohli, P.; Sanjesh, J. Liposome-Mesoporous Silica Nanoparticles Fused Cores: A Safer Mode of Drug Carrier. *J. Biomed. Nanotechnol.* **2011**, *7*, 60–62.
27. María, V.-R.; Montserrat, C.; Isabel, I.-B. Bioactive Mesoporous Silicas As Controlled Delivery Systems: Application in Bone Tissue Regeneration. *J. Biomed. Nanotechnol.* **2008**, *4*, 1–15.
28. Qu, F. Y.; Zhu, G. S.; Lin, H. M.; Zhang, W. W.; Sun, J. Y.; Li, S. G.; Qiu, S. L. Controlled Release of Captopril by Regulating the Pore Size and Morphology of Ordered Mesoporous Silica. *J. Solid State Chem.* **2006**, *179*, 2027–2035.
29. Muthu, M. S.; Rajesh, C. V.; Mishra, A.; Singh, S. Stimulus-Responsive Targeted Nanomicelles for Effective Cancer Therapy. *Nanomedicine (London, U. K.)* **2009**, *4*, 657–667.
30. Gou, M. L.; Zheng, X. L.; Men, K.; Zhang, J.; Zheng, L.; Wang, X. H.; Luo, F.; Zhao, Y. L.; Zhao, X.; Wei, Y. Q.; *et al*. Poly(ε-caprolactone)/Poly(ethylene glycol)/Poly(ε-caprolactone) Nanoparticles: Preparation, Characterization, and Application in Doxorubicin Delivery. *J. Phys. Chem. B* **2009**, *113*, 12928–12933.
31. Vora, J.; Bapat, N.; Boroujerdi, M. Investigation of the Relative Affinity of Doxorubicin for Neutral and Negatively Charged Particulate Carriers. *Drug Dev. Ind. Pharm.* **1993**, *19*, 759–771.
32. Meng, H.; Liong, M.; Xia, T.; Li, Z.; Ji, Z.; Zink, J. I.; Nel, A. E. Engineered Design of Mesoporous Silica Nanoparticles to Deliver Doxorubicin and P-glycoprotein siRNA to Overcome Drug Resistance in a Cancer Cell Line. *ACS Nano* **2010**, *4*, 4539–4550.
33. Li, L.; Guan, Y.; Liu, H.; Hao, N.; Liu, T.; Meng, X.; Fu, C.; Li, Y.; Qu, Q.; Zhang, Y.; *et al.* Silica Nanorattle-doxorubicin-anchored Mesenchymal Stem Cells for Tumor-tropic Therapy. *ACS Nano* **2011**, *5*, 7462–7470.
34. Song, M.; Wang, X.; Li, J.; Zhang, R.; Chen, B.; Fu, D. Effect of Surface Chemistry Modification of Functional Gold Nanoparticles on the Drug Accumulation of Cancer Cells. *J. Biomed. Mater. Res. A* **2008**, *86*, 942–946.
35. Chen, B.; Cheng, J.; Shen, M.; Gao, F.; Xu, W.; Shen, H.; Ding, J.; Gao, C.; Sun, Q.; Sun, X.; *et al.* Magnetic Nanoparticles of Fe_3O_4 and 5-Bromotetrandrin Interact Synergistically to Induce Apoptosis by Daunorubicin in Leukemia Cells. *Int. J. Nanomed.* **2009**, *4*, 65–71.
36. Li, R.; Wu, R.; Zhao, L.; Wu, M.; Yang, L.; Zou, H. P-Glycoprotein Antibody Functionalized Carbon Nanotube Overcomes the Multidrug Resistance of Human Leukemia Cells. *ACS Nano* **2010**, *4*, 1399–1408.
37. Liang, X. J.; Chen, C.; Zhao, Y.; Wang, P. C. Circumventing Tumor Resistance to Chemotherapy by Nanotechnology. *Methods Mol. Biol.* **2010**, *596*, 467–488.
38. Chen, Y.; Chen, H. R.; Guo, L. M.; He, Q. J.; Chen, F.; Zhou, J.; Feng, J. W.; Shi, J. L. Hollow/Rattle-Type Mesoporous Nanostructures by a Structural Difference-Based Selective Etching Strategy. *ACS Nano* **2010**, *4*, 529–539.